Progress In Electromagnetics Research C, Vol. 90, 95–107, 2019

A Novel Design of Hybrid Open Slot Antenna with Parasitic Element for Wideband Applications

Prashant Purohit*, Bhupendra K. Shukla, and Deepak K. Raghuvanshi

Abstract—In this communication, a novel design of a hybrid open slot antenna is investigated and experimentally verified. The proposed structure comprises a slotted tuning stub, a proximity fed parasitic element, and slotted ground plane. Tuning and overlapping of best matching frequencies f_{r1}, f_{r2}, f_{r3}, f_{r4}, f_{r5}, f_{r6}, and f_{r7} are accomplished by varying the dimension of the parasitic element and elliptical slot. The experimental results reveal that this antenna covers the fractional bandwidth (BW(%) $= 200 * (f_h - f_l)/(f_h + f_l)$) of 139.5% from 0.98 GHz to 5.5 GHz for $|S_{11}| < -10$ dB which is suitable for GSM 1800, WiMAX, PCS, and ITM-2000. After the analysis of current distribution, mathematical equations are developed for frequencies 1.04, 1.52, 3.06, 3.67, and 4.58 GHz. The structural analysis is also carried out for optimization and to know the electromagnetic behaviour of the antenna. Asymmetric radiation patterns are found at resonating frequencies due to open slot geometry.

1. INTRODUCTION

Printed open slot antennas become popular in the wireless communication industry due to their compactness, impedance bandwidth, the capability to produce linear and circular polarization, and far field characteristics. Moreover, they also offer features like conventional microstrip patch antennas [1, 2]. Due to quarter wave resonance ($\lambda/4$), the sizes of open slot antennas are smaller than wide slot antennas [3]. The core functions of slots are 1) modify the path length of current vectors, 2) change the equivalent capacitance of the antenna, 3) alter the position of modes (TM_{10}, TM_{01}, TM_{12} and TM_{20}), 4) change the phase velocity ($v_p = 1/\sqrt{LC}$) of the resonating frequencies. In addition, slot loaded antenna exhibits a large number of resonating modes (f_{r1}, f_{r2}, f_{r3}, f_{r4}, f_{r5}, f_{r6}, and f_{r7}) (as shown in Figure 1(a)). By choosing an appropriate dimension of the antenna, the overlapping of these modes (as shown in Figure 1(b)) can be achieved, and wide impedance bandwidth is achieved [4–6]. By introducing notches on the L shaped open slot, the resonant path length can be varied which directly affects the impedance bandwidth of the antenna [3]. Reshaping the open slot affects the bandwidth of the antenna and position of lower and higher cutoff frequencies [7–9]. Rotation of the radiating structure changes the position of resonating modes. By choosing a suitable angle, the bandwidth can be improved [10]. Reshaping the feed structure and radiating element are also techniques to enhance the bandwidth of an open slot antenna [11–14]. Tuning stub performs the operation of overlapping of resonating modes. By integrating a tuning stub with radiating element, wide bandwidth can be realized [15]. In this article, we present a novel design of a hybrid open slot antenna with proximity fed parasitic element for wide band applications (GSM 1800, WiMAX, PCS and ITM-2000). The hybrid open slot geometry is obtained after the integration of elliptical and rectangular shaped slots. The proposed structure occupies the impedance bandwidth of 139.5% for $|S_{11}| < -10$ dB that covers the frequency range from 0.98 GHz to 5.5 GHz. The input impedance behaviour of this antenna is also analyzed. At best matching frequencies,

Received 1 November 2018, Accepted 13 January 2019, Scheduled 27 February 2019
* Corresponding author: Prashant Purohit (prashantpurohit.manit@gmail.com).
The authors are with the Maulana Azad National Institute of Technology, Bhopal, India.

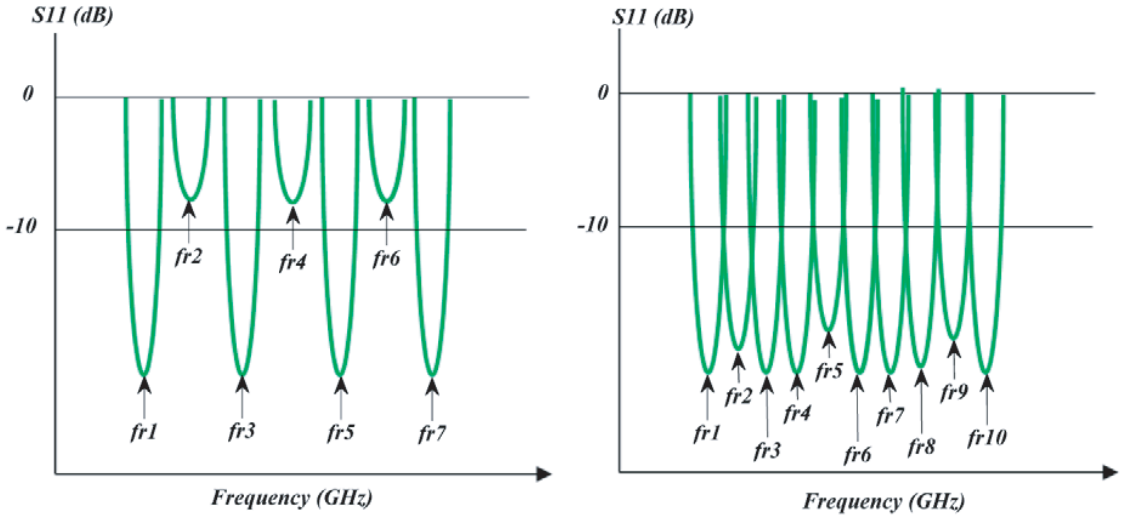

Figure 1. Impedance characteristic of the slot loaded antenna. (a) Before tuning. (b) After tuning of modes.

the surface current distribution is investigated, and the mathematical model has been developed. The effect of the key parameters on the $|S_{11}|$ characteristic and bandwidth are investigated. Finally, the far field characteristic of the antenna is measured and compared with the simulated results.

2. ANTENNA CONFIGURATION

The two-dimensional geometry and parameters of the proposed hybrid open slot antenna with proximity fed parasitic element are illustrated in Figure 2, which is placed on the $Z = 0$ plane. In the simulation, we have taken 0.035 mm thin conducting layers. A 50 Ω microstrip feed line ($M_w \times M_l$) is designed on the top layer of an FR-4 substrate ($\tan(\delta) = 0.02$, $\varepsilon_r = 4.3$ and $h = 1.6$ mm) which is terminated on the elliptical shaped tuning stub with variables R_{l1} (semi minor axis radius) and R_{w1} (semi major axis

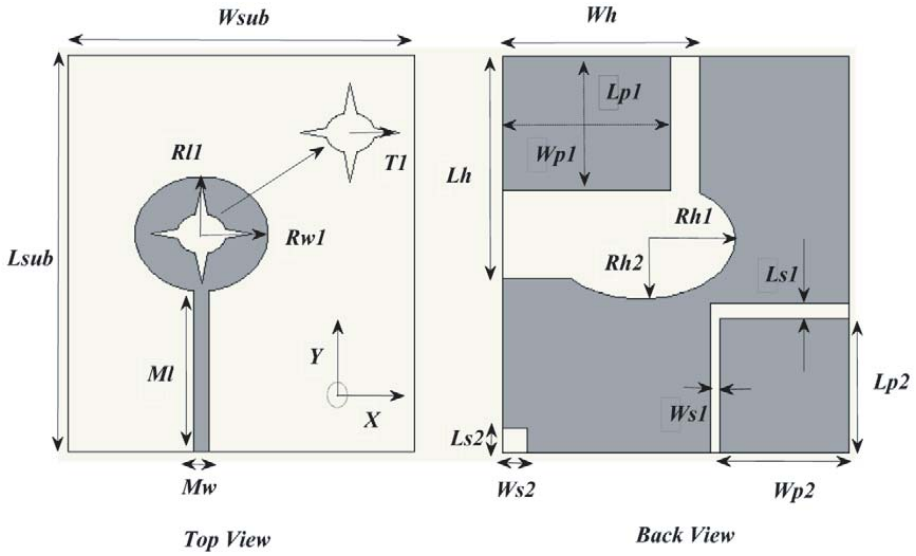

Figure 2. Configuration of the propose hybrid open slot antenna with proximity fed parasitic element.

radius). Moreover, a hybrid slot which is the union of four triangular slots is loaded on the stub for bandwidth enhancement. On the bottom side of the substrate, the ground plane has been printed with the parameters of L_{sub} and W_{sub}. For performance improvement, a composite slot is embedded on the ground plane. This hybrid slot is made after the combination of a rectangular shaped slot ($L_h \times W_h$) and elliptical slot (R_{h1} (semi minor axis radius) and R_{h2} (semi major axis radius)). The size of the elliptical slot plays a vital role in impedance matching which will be discussed later. For overlapping of resonating modes, a rectangle-shaped parasitic element ($L_{p1} \times W_{p1}$) is integrated on the bottom layer. An L-shaped slot is etched on the right bottom side of the ground plane which is also responsible for tuning of modes. In addition, a small rectangular slot ($L_{s2} \times W_{s2}$) is also Boolean subtracted at the left bottom corner of the ground plane. Table 1 represents the chosen dimension of the proposed antenna after the parametric study.

Table 1. The proposed dimension of the hybrid open slot antenna with proximity fed parasitic element.

Parameter	Dimension (mm)	Parameter	Dimension (mm)	Parameter	Dimension (mm)	Parameter	Dimension (mm)
M_w	3	W_{sub}	70	R_{h2}	12	R_{h1}	19
M_l	33.5	L_h	45	L_{s1}	3	W_{p2}	26
R_{l1}	11.5	W_h	40	W_{s1}	2	L_{p2}	27
R_{w1}	13.5	L_{p1}	27	W_{s2}	5	L_{s2}	5
T_1	10	W_{p1}	34	L_{sub}	80		

3. EVOLUTION OF ANTENNA

Evolution of the proposed antenna is shown in Figure 3. In succeeding stages, the ground plane and tuning stub are modified for bandwidth enhancement and proper tuning of the resonating modes. The comparison of reflection coefficient characteristics of all stages is depicted in Figure 4. Antenna 1

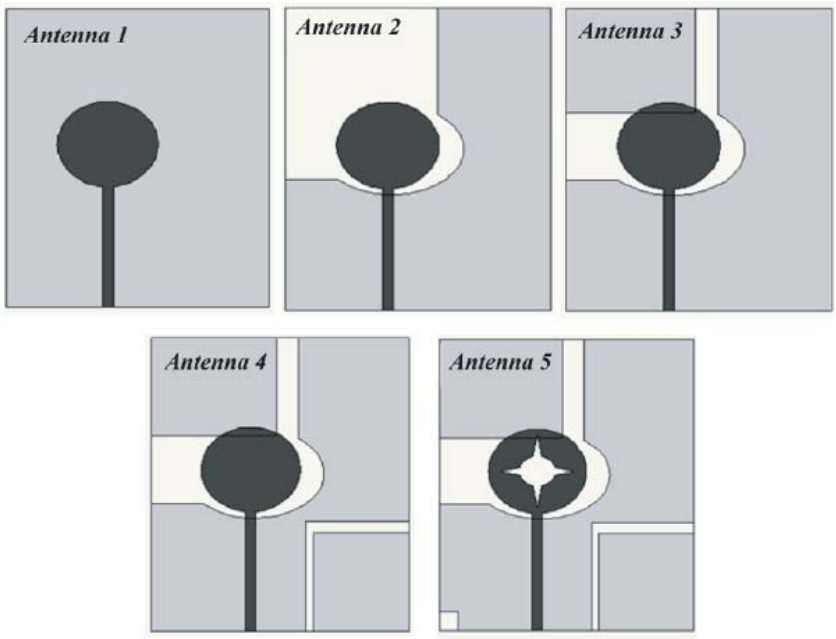

Figure 3. Schematic of development of the hybrid open slot antenna with proximity fed parasitic element.

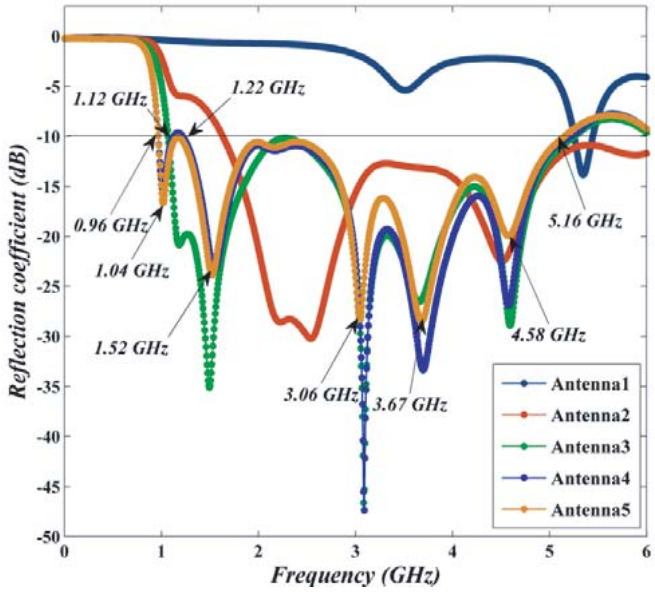

Figure 4. Comparison of reflection coefficient characteristics of antenna 1, 2, 3, 4, and 5.

comprises a full ground plane and an elliptical shaped tuning stub. This antenna exhibits single band response and resonates at 5.2 GHz.

The behavior of Antenna 1 is similar to the conventional microstrip antenna which shows narrow impedance bandwidth. Further, a hybrid slot is etched on the ground plane which introduces slow wave effect [9]. This composite slot has two functions i) Impedance matching, ii) Overlapping of resonating modes. Antenna 2 covers the frequency range from 1.7 GHz to 6 GHz and exhibits the bandwidth of 111.68% for $|S_{11}| < -10$ dB with three best matching frequencies 2.19, 2.53, and 4.51 GHz. In Antenna 3, a rectangle-shaped parasitic element is integrated in the ground plane which improves the mutual coupling between radiating patch and hybrid slot. This parasitic element also improves the impedance matching in the lower frequency band. It exhibits the bandwidth of 132.038% for $|S_{11}| < -10$ dB and covers the frequency range from 1.068 to 5.25 GHz with five best matching frequencies 1.18, 1.49, 3.08, 3.65, and 4.59 GHz. For impedance matching in the lower frequency band, the L-shaped slot is truncated on the right bottom side of the ground plane. Slot enhances the path length of the current which reduces the frequency of the resonating modes [4, 5]. Antenna 4 covers the bandwidth of 137.45% from 0.96 to 5.16 GHz for $|S_{11}| < -10$ dB with one notched frequency band from 1.12 to 1.22 GHz. It resonates at five frequencies 1.04 GHz, 1.52 GHz, 3.06 GHz, 3.67 GHz, and 4.58 GHz. In the final step, to suppress the notched frequency band, a hybrid slot on tuning stub and rectangle-shaped slot on ground plane are incorporated. These slots also affect the impedance matching at resonating frequencies 3.06 GHz, 3.67 GHz, and 4.58 GHz. Antenna 5 covers the bandwidth of 137.45% from 0.96 to 5.16 GHz for $|S_{11}| < -10$ dB.

4. TUNING OF PARAMETERS

To know the effect of key parameters on bandwidth and impedance matching, the parameters are varied in a specified range. In this section, we study the drift of best matching frequency due to the tuning of parameters. In this study, only a single parameter is varied at a time.

4.1. Influence of Parameters (R_{h1} and R_{h2}) of the Elliptical Slot

The impact of R_{h1} (major axis radius of the elliptical slot) and R_{h2} (minor axis radius of the elliptical slot) on $|S_{11}|$ characteristic of the proposed antenna is illustrated in Figure 5. It is noticed that by increasing R_{h1}, the lower cutoff frequency (f_l), fundamental frequency resonating (f_{r1}), second

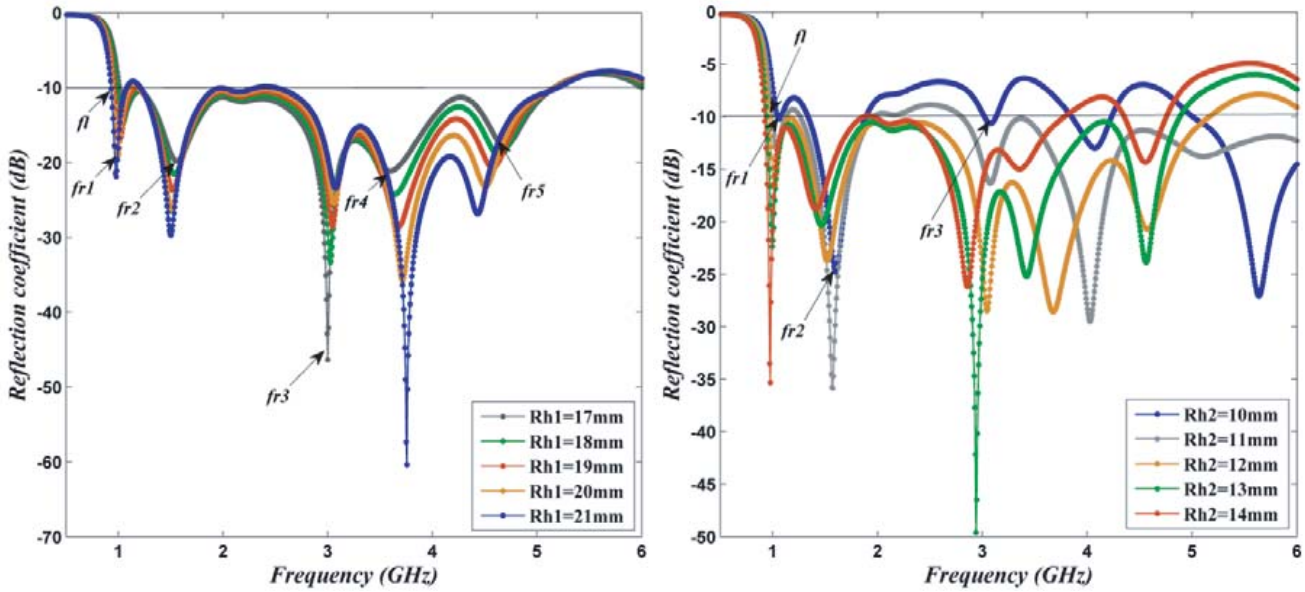

Figure 5. Simulated reflection coefficient characteristic versus frequency for different value of $\boldsymbol{R_{h1}}$ and $\boldsymbol{R_{h2}}$ of the proposed antenna.

resonating frequency (f_{r2}), and fifth resonating frequency (f_{r5}) are drifted in a leftward direction. Increment in R_{h1} increases the equivalent capacitance of the antenna which reduces the phase velocity of f_l, f_{r1}, f_{r2}, and f_{r5}. In addition, for higher value of $R_{h1} > 19\,\text{mm}$, the impedance matching is reduced in lower and mid-frequency band. A good impedance bandwidth is obtained for $R_{h1} = 19\,\text{mm}$. Apart from this, the resonating frequencies f_{r3} and f_{r4} are shifted in rightward direction, and impedance matching is increased at f_{r4} while decreasing at f_{r3}. With increasing the value of R_{h2}, the slot area of the ellipse also increases which enhances the path length of the current vectors. Due to increment in path length, f_l, f_{r1}, and f_{r2} shift in a leftward direction. Moreover, the impedance matching is improved at frequency f_{r3} due to the capacitive coupling between slot and tuning stub. It is also noticed that the impedance matching is improved at lower frequency band while it decreases at higher frequency band with increasing the value of R_{h2}. The maximum bandwidth is found for $R_{h2} = 12\,\text{mm}$.

4.2. Influence of Parameter (L_{p1} and W_{p1}) of the Parasitic Element

The impact of L_{p1} (length of the parasitic element) on $|S_{11}|$ characteristic of the proposed antenna is depicted in Figure 6. It is clear from the figure that with increasing the length of the parasitic element, the impedance matching is improved on lower frequency band while it is deteriorated in the frequency band near 2 GHz. Moreover, this parameter slightly affects the position of higher cutoff frequency (f_h) which is shifted in leftward direction. In addition, impedance matching at the fundamental frequency (f_{r1}) and second resonating frequency f_{r2} is improved while it is decreased at frequencies f_{r3} and f_{r6}. The resonance frequency f_{r2} is drifted in a leftward direction due to increment in equivalent capacitance of the antenna. Uneven impedance matching is noticed at frequency f_{r4}. The maximum bandwidth of the antenna is obtained for $L_{p1} = 27\,\text{mm}$. The influence of the width of the parasitic element is also displayed in Figure 6. It is noticed that the impedance matching is improved with increasing the value of W_{p1} which indicates that the mutual coupling between open slot and tuning stub is improved by W_{p1}. The maximum bandwidth is obtained for $W_{p1} = 34\,\text{mm}$. The resonance frequencies f_{r2} and f_{r4} are drifted in left direction while frequencies f_{r3} and f_{r5} are shifted towards higher frequency band. The left shift of higher cutoff frequency is also observed. The shift of resonance frequencies is noticed in the frequency spectrum due to the change in equivalent capacitance of the antenna which directly affects the phase velocity of the resonating modes.

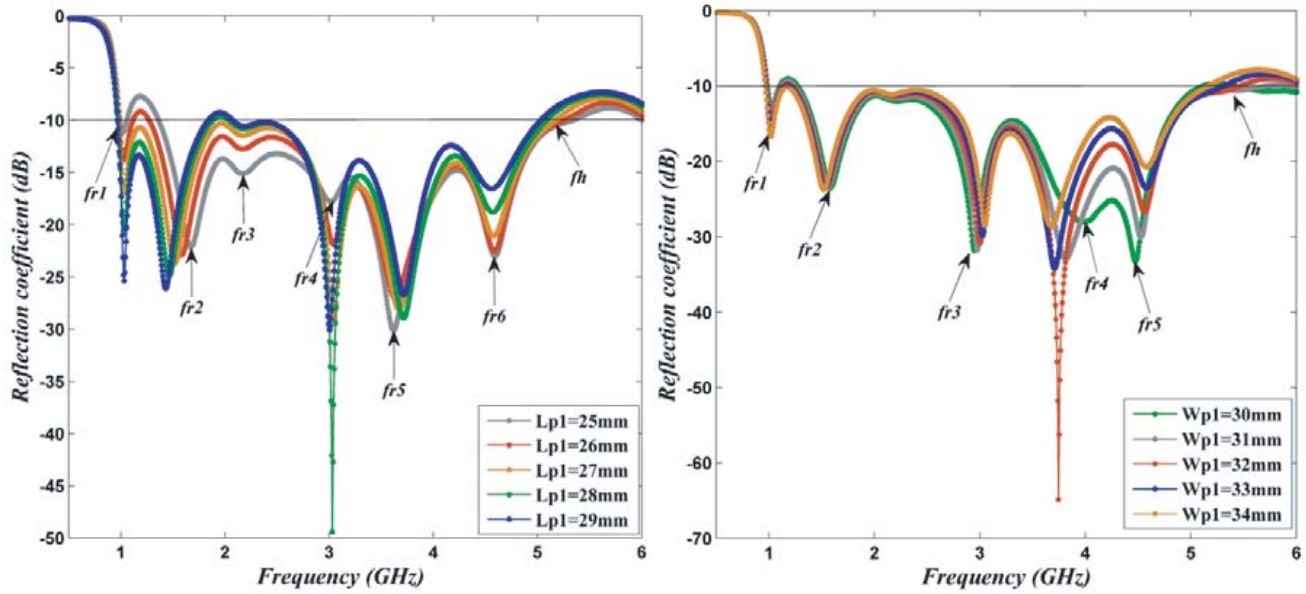

Figure 6. Simulated reflection coefficient characteristic versus frequency for different length and width of the parasitic element.

4.3. Influence of Parameter (L_{s1} and W_{s1}) of the L-Shaped Slot

The effect of L_{s1} on $|S_{11}|$ parameter of the proposed antenna is displayed in Figure 7. This parameter slightly affects the position of the lower cutoff frequency and first resonating frequency. With increasing parameter L_{s1}, the positions of f_l and f_{r1} are shifted in rightward direction. Slot modifies the equivalent capacitance of the antenna which enhances the phase velocity of resonating modes. The optimized value of L_{s1} is 3 mm because this value offers the maximum bandwidth. In addition, impedance matchings at frequencies f_{r1}, f_{r3} and f_{r5} are enhanced while they are decreased at frequencies f_{r2} and f_{r4}. Parameter

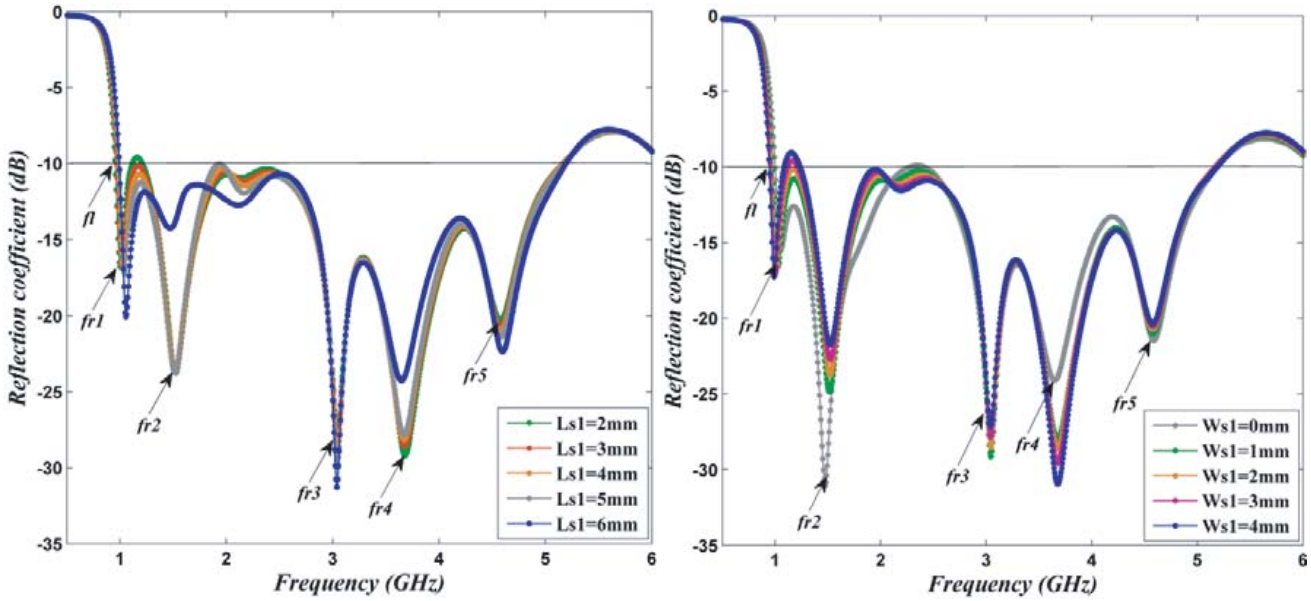

Figure 7. Simulated reflection coefficient characteristic versus frequency for the different length of the L shaped slot.

W_{s1} mainly affects the position of lower cutoff frequency and impedance matching in lower and mid frequency band. With increasing W_{s1}, the lower cutoff frequency is shifted towards the lower frequencies while impedance matching becomes poor in the lower frequency band. The optimized value of W_{s1} is 2 mm.

5. EXPERIMENTAL RESULTS AND DISCUSSION

5.1. Reflection Coefficient Characteristic

In this section, the reflection coefficient characteristic and input impedance of the proposed antenna are discussed. The numerical analysis of the antenna is achieved by CST Microwave Studio. The structure is excited by waveguide port with height 12.96 mm and width 25.72 mm. After the simulation and optimization of the dimension of the antenna, the proposed structure is manufactured on an FR-4 substrate. The pictorial view of the fabricated hybrid open slot antenna with a proximity fed parasitic element is displayed in Figure 8.

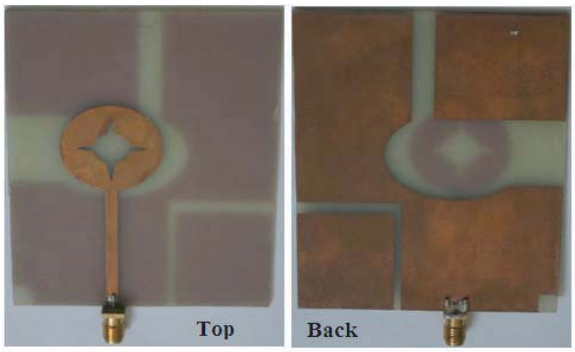

Figure 8. Configuration of fabricated hybrid open slot antenna with proximity fed parasitic element.

The experimental results such as reflection coefficient characteristic and input impedance are obtained from Agilent Technologies based Vector Network Analyzer N2223A in the frequency span 0.8 to 6 GHz. The compared reflection coefficient characteristics of the proposed antenna are illustrated in Figure 9. It has been noticed that the lower cutoff frequency of this antenna depends on the dimension of the hybrid slot which is truncated on the ground plane. The mathematical equation for lower cutoff frequency is deduced after inspecting the current distribution at frequency 1.04 GHz (see Figure 11).

$$L_{flc} = L_1 + L_2 + L_3 + L_4 + L_e/2 \quad (1)$$

$$L_1 = L_{sub} - L_h + W_{s2} \quad (2)$$

$$L_e \cong 2\pi\sqrt{(R_{h2}^2 + R_{h2}^2)/2} \quad (3)$$

$$f_{lc} = \frac{c}{L_{flc}\sqrt{\varepsilon_r}} \quad (4)$$

where c and ε_r are the speed of light and permittivity of the substrate, respectively. From Equation (4), the calculated value of lower cutoff frequency is 0.9 GHz. An error of 8.16% is computed between measured and simulated lower cutoff frequencies. The proposed antenna shows the bandwidth (measured) of 139.5% from 0.98 GHz to 5.5 GHz for $|S_{11}| < -10$ dB. It also exhibits the resonances at frequencies (measured) 1.12, 1.82, 2.8, 3.1, 3.67, 4.5, and 5.1 GHz. A mismatch between measured and simulated results has been found due to SMA connector and fabrication tolerance. Another cause of inaccuracy is a variation of dielectric constant.

5.2. Input Impedance

Figure 10 illustrates the comparison (simulated and measured) of the real and imaginary part of the input impedance (Z_{in}) which is the function of frequency. It is noticed that resistance (measured) is

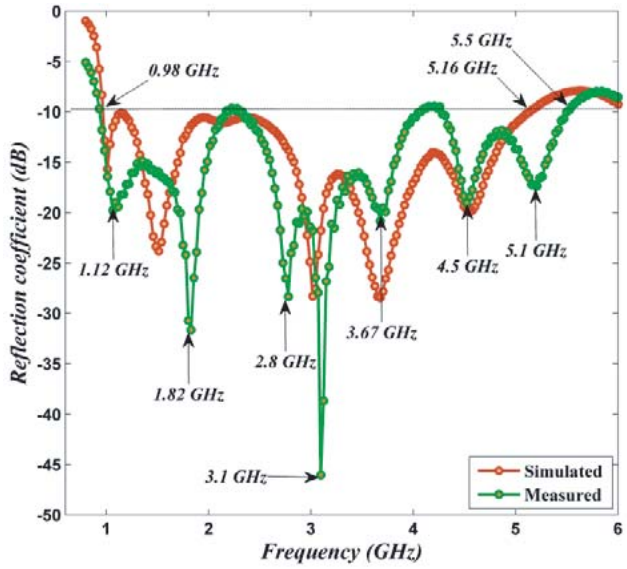

Figure 9. Comparison of simulated and measured reflection coefficient versus frequency plots.

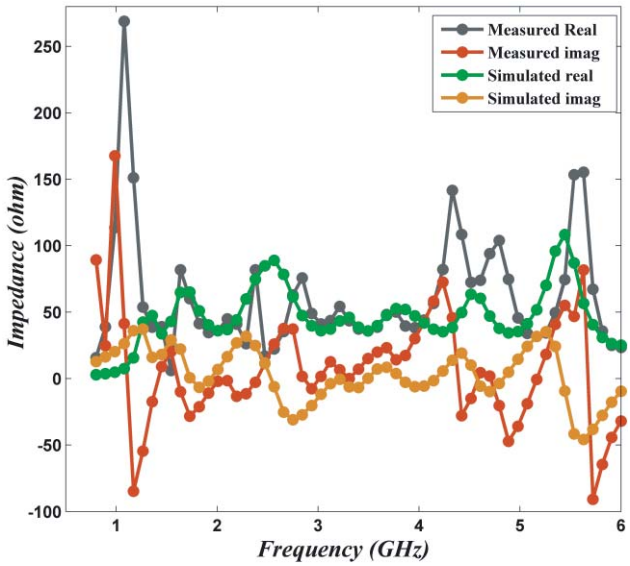

Figure 10. Comparison of simulated and measured input impedance versus frequency plots.

higher in the lower and higher frequency bands than simulated resistance. The simulated and measured resistances oscillate around 50 Ω. The maximum peak of measured resistance is 270 Ω. The measured reactance of the antenna varies between 170 Ω and −80 Ω. As shown in Figure 10, the simulated imaginary part of the input impedance oscillates around 0 Ω.

6. SURFACE CURRENT DISTRIBUTION AND FAR-FIELD PATTERNS

The simulated vector current distributions at frequencies 1.04 GHz, 1.52 GHz, 3.06 GHz, 3.67 GHz, and 4.58 GHz are displayed in Figure 11. The current vectors are scattered on the tuning stub, parasitic element and ground plane. At first resonating frequency ($f_1 = 1.04$ GHz), the maximum strength of the current is found along the hybrid slot which is embedded in the ground plane. This frequency is produced due to the side edge of the ground plane and can be determined by following Equations (5)–(10).

$$L_{f1} = L_5 + L_6 + L_7 + L_8 \tag{5}$$

$$L_5 = W_{sub} - W_{p2} - W_{s2} - W_{s1} \tag{6}$$

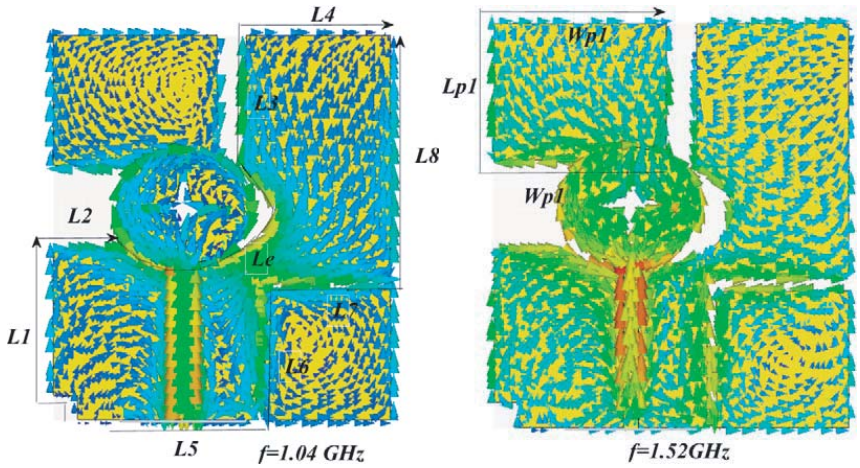

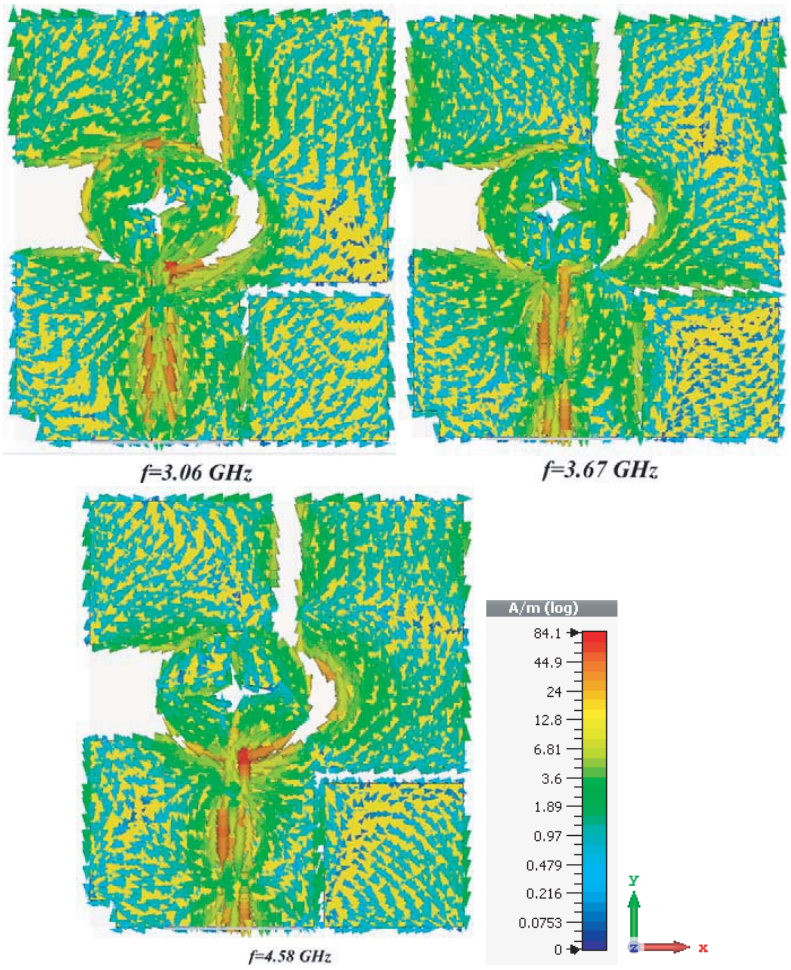

Figure 11. Surface current distribution at frequency 1.04, 1.52, 3.06, 3.67 and 4.58 GHz.

$$L_6 = L_{p2} + L_{s1} \tag{7}$$

$$L_7 = W_{s1} + W_{p2} \tag{8}$$

$$L_8 = L_{sub} - L_{s1} - L_{p2} \tag{9}$$

$$f_1 = \frac{c}{L_{f1}\sqrt{\varepsilon_r}} \tag{10}$$

The computed length of L_{f1} is 135 mm, and the calculated value of f_1 is 1.06 GHz (using Equation (10)) which is nearly equal to 1.04 GHz. An error between the simulated and calculated values of the first resonating frequency is 1.88%. At the second resonating frequency (f_2), the current vectors are distributed along the circumference of the parasitic element. After inspection, it is noticed that this resonance frequency is developed due to the parasitic element and can be determined by following equations.

$$L_{f2} = 2 * W_{p1} + L_{p1} \tag{11}$$

$$f_2 = \frac{c}{L_{f2}\sqrt{\varepsilon_r}} \tag{12}$$

The computed length of L_{f2} is 95 mm, and the calculated value of f_2 is 1.51 GHz (using Equation (12)) which is nearly equal to 1.52 GHz. An error between the simulated and calculated values of the second resonating frequency is 0.65%. At frequency 3.06 GHz, one half wave variations of current vectors are investigated along the elliptical slot which is etched on the ground plane. This resonating frequency is

developed due to the elliptical slot and can be calculated by the following equations

$$L_{f3} = L_e/2 \tag{13}$$

$$f_3 = \frac{c}{L_{f3}\sqrt{\varepsilon_r}} \tag{14}$$

where L_e is the total circumference length of the elliptical slot. The computed value of L_{f3} is 49.89 mm, and the calculated value of f_3 is 2.88 GHz. An error between the simulated and calculated values of the third resonating frequency is 5.88%. The resonating frequency f_4 (3.67 GHz) is developed due to the elliptical shaped tuning element. At this frequency (f_4), one half wave variations of current vectors are investigated along the elliptical patch, and this frequency can be calculated by following equations

$$L_{e1} \cong \pi\sqrt{(R_{l1}^2 + R_{w1}^2)/2} \tag{15}$$

$$f_4 = \frac{2c}{L_{e1}\sqrt{\varepsilon_r}} \tag{16}$$

where L_{e1} is the half circumference length of the elliptical shaped tuning element. The calculated value of L_{e1} is 39.37 mm, and the calculated value of f_4 is 3.64 GHz (using Equation (16)). An error

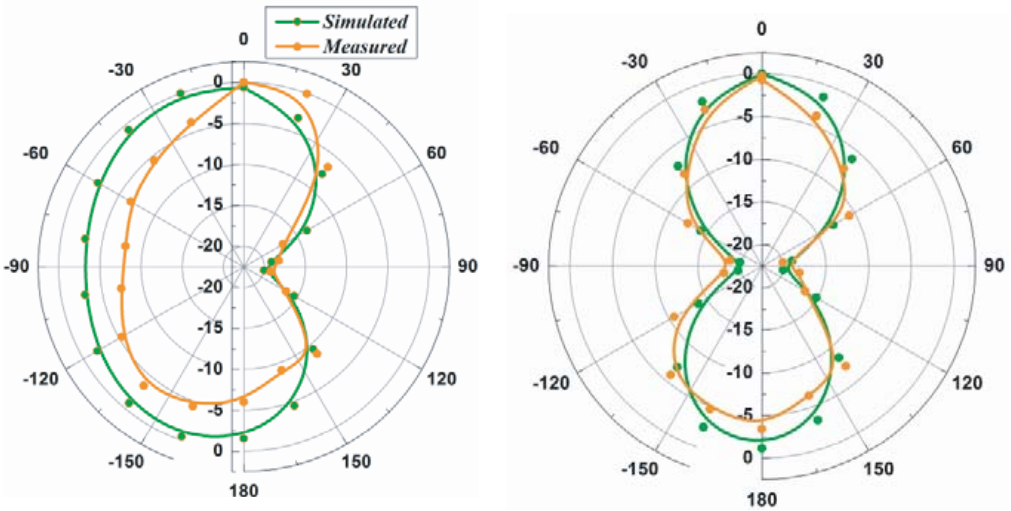

(1.04 GHz)

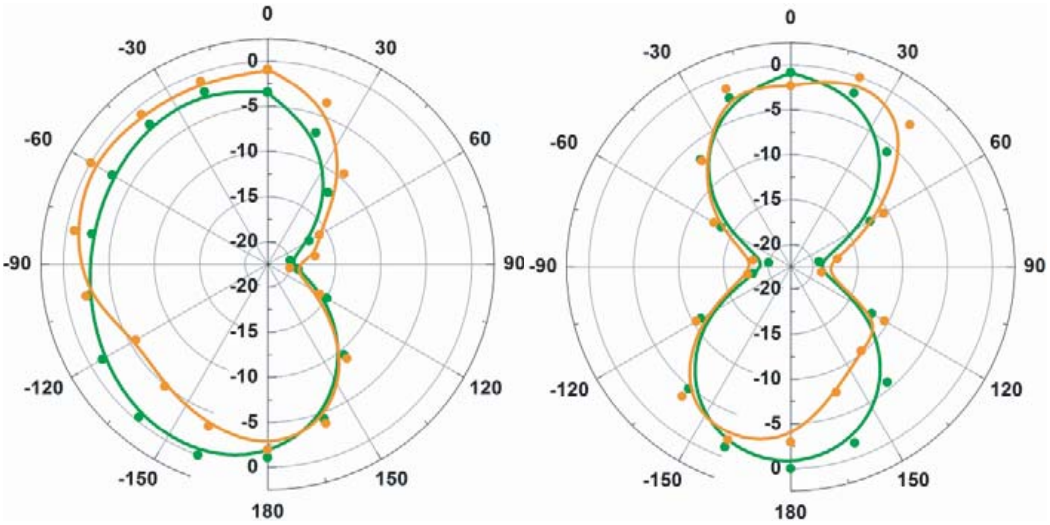

(1.52 GHz)

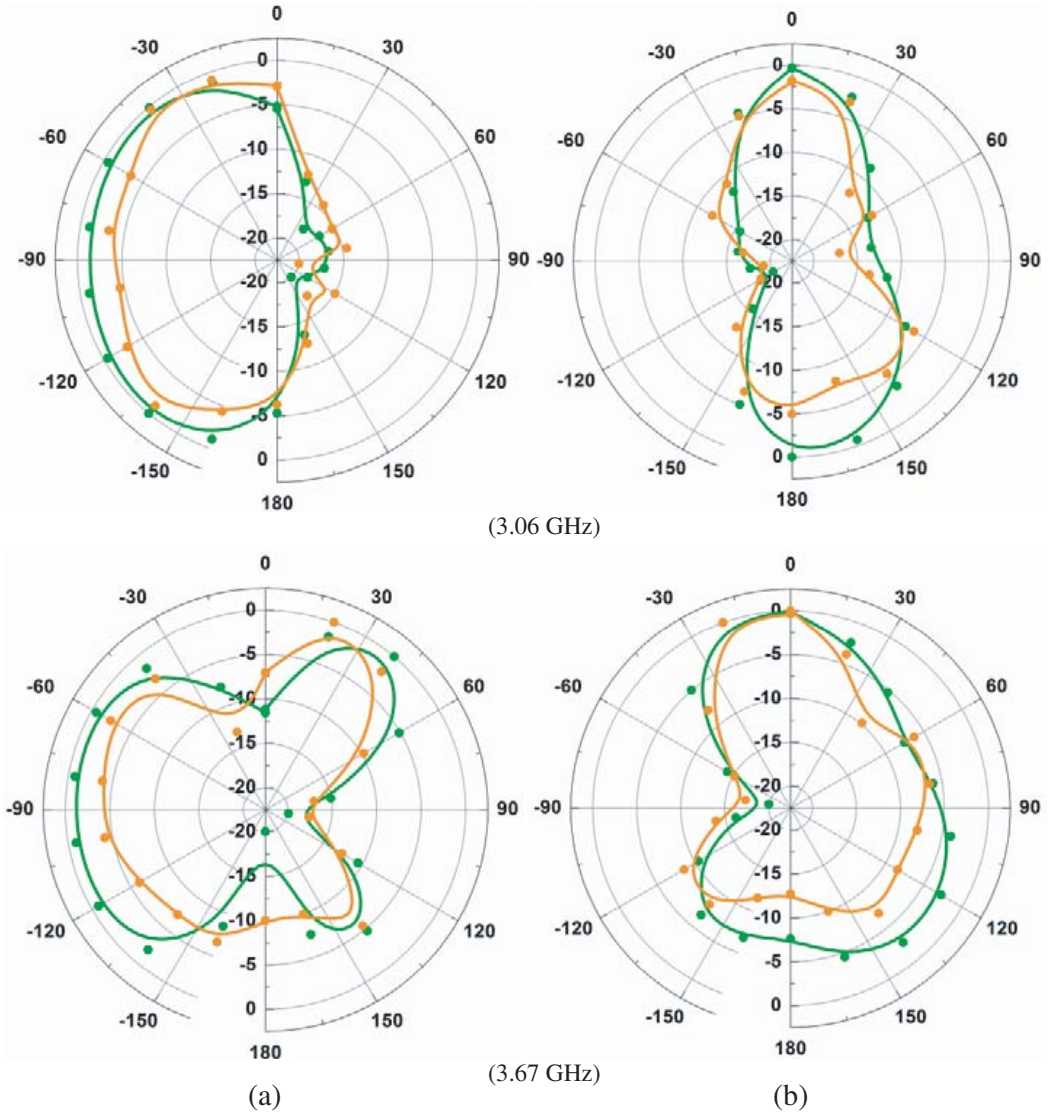

Figure 12. (a) E plane and (b) H plane pattern at frequencies $f_1 = 1.04\,\text{GHz}$, $f_2 = 1.52\,\text{GHz}$, $f_3 = 3.06\,\text{GHz}$ and $f_4 = 3.67\,\text{GHz}$.

between the simulated and calculated values of the fourth resonating frequency is 0.81%. At frequency f_5 (4.58 GHz), complicated current distributions are investigated which indicates the presence of higher order modes. At this frequency (f_5), multiple variations of current vectors are analyzed along elements of the antenna. Figure 12 exhibits the compared far field pattern at resonating frequencies 1.04, 1.52, 3.06, and 3.67 GHz. E plane patterns are asymmetric due to asymmetry in the ground plane. At frequencies 1.04 and 1.52 GHz, an eight-shaped pattern is observed in H-plane while the eight-shaped pattern is changed at frequencies 3.06 and 3.67 GHz due to the existence of higher order modes. Measured patterns slightly differ from the simulated pattern because of measurement and fabrication error. The gain and efficiency of the proposed antenna are exhibited in Figure 13. The antenna gain is calculated at frequencies 1.04, 1.52, 3.06, and 3.67 GHz. The simulated realized gain is varied between 2.1 and 5.2 dBi. It is noticed that the efficiency of the antenna is decreased as operating frequency increases.

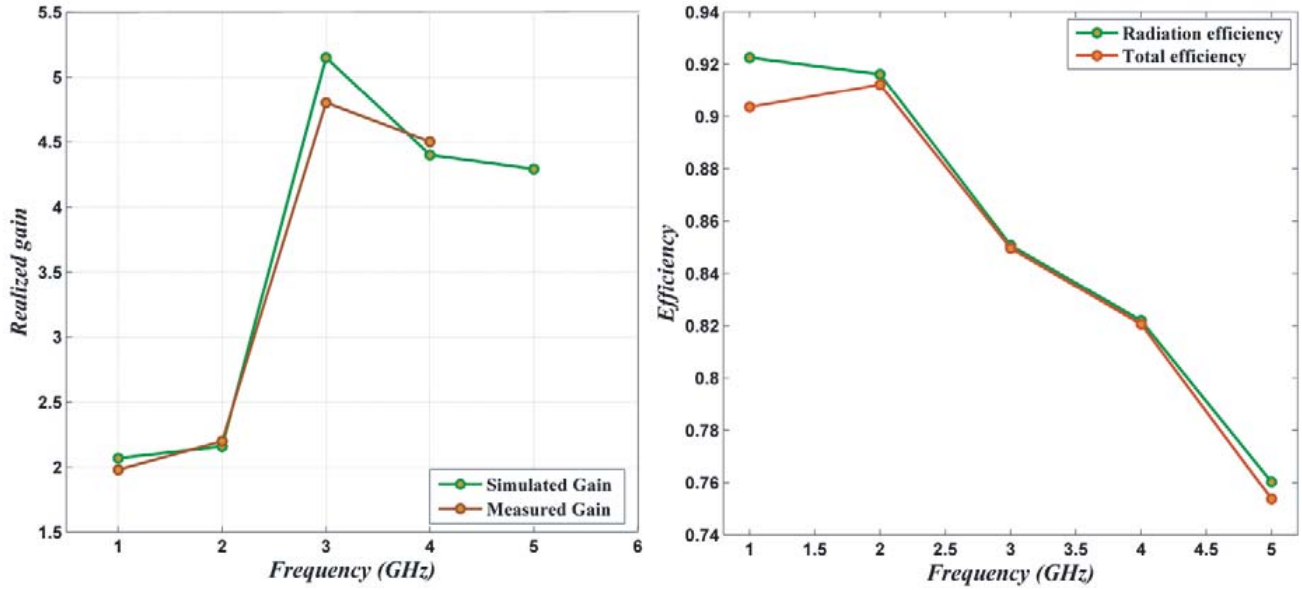

Figure 13. The realized gain and simulated efficiency of the proposed antenna.

7. CONCLUSION

A hybrid open slot antenna with proximity fed parasitic element is numerically analyzed, fabricated, and experimentally verified for wideband applications. It has been found that parameters of the elliptical slot and L-shaped slot play an important role in impedance matching and bandwidth. The proposed antenna covers the bandwidth of 139.5% from 0.98 GHz to 5.5 GHz for $|S_{11}| < -10$ dB. This antenna is suitable for GSM 1800, WiMAX, PCS, and ITM-2000 applications. At best matching frequencies 1.04 GHz, 1.52 GHz, 3.06 GHz, 3.67 GHz, and 4.58 GHz, the surface current distribution is investigated, and the mathematical model is developed for each resonating frequency. The far field pattern is analyzed in both planes. The asymmetry in radiation pattern is due to asymmetric open slot configuration, and the shape of the pattern is changed due to higher order modes at higher frequencies.

REFERENCES

1. Wang, C. J., M. H. Shih, and L. T. Chen, "A wideband open-slot antenna with dual-band circular polarization," *IEEE Antennas and Wireless Propagation Letters*, Vol. 14, 1306–1309, 2015.
2. Wang, C. J. and W. B. Tsai, "Microstrip open-slot antenna with broadband circular polarization and impedance bandwidth," *IEEE Transactions on Antennas and Propagation*, Vol. 64, 4095–4098, 2016.
3. Chen, W. S. and K. Y. Ku, "Bandwidth enhancement of open slot antenna for UWB applications," *Microwave and Optical Technology Letters*, Vol. 50, 438–439, 2008.
4. Deshmukh, A. A. and K. P. Ray, "Compact broadband slotted rectangular microstrip antenna," *IEEE Antennas and Wireless Propagation Letters*, Vol. 8, 1410–1413, 2009.
5. Deshmukh, A. A. and K. P. Ray, "Analysis of broadband variations of U-slot cut rectangular microstrip antennas," *IEEE Antennas and Propagation Magazine*, Vol. 57, 181–193, 2015.
6. Tang, M. C., R. W. Ziolkowski, and S. Xiao, "Compact hyper band printed slot antenna with stable radiation properties," *IEEE Transactions on Antennas and Propagation*, Vol. 62, No. 6, 2962–2969, Jun. 2014.
7. Wang, C. J. and C. M. Lin, "A CPW-fed open-slot antenna for multiple wireless communication systems," *IEEE Antennas and Wireless Propagation Letters*, Vol. 11, 620–623, 2012.

8. Deng, J. Y., T. Q. Fan, Y. Zhang, X. Wen, G. Q. Liu, and L. X. Guo, "An open slot antenna with bandwidth extension for WLAN/UWB applications," *International Journal of Antennas and Propagation*, 1–7, 2015.
9. Al-Azza, A. A., F. J. Harackiewicz, and H. R. Gorla, "Very compact open-slot antenna for wireless communication systems," *Progress In Electromagnetics Research Letters*, Vol. 51, 73–78, 2015.
10. Song, K., Y.-Z. Yin, B. Chen, S.-T. Fan, and F. Gao, "Bandwidth enhancement design of compact UWB step-slot antenna with rotated patch," *Progress In Electromagnetics Research Letters*, Vol. 22, 39–45, 2011.
11. Su, M., Y. A. Liu, S. L. Li, and C. P. Yu, "A compact open slot antenna for uwb applications with band-notched characteristic," *Journal of Electromagnetic Waves and Applications*, Vol. 24, 2001–2010, 2010.
12. Jan, J. Y., C. Y. Pan, K. Y. Chiu, and H. M. Chen, "Broadband CPW-fed circularly-polarized slot antenna with an open slot," *IEEE Transactions on Antennas and Propagation*, Vol. 61, 1418–1422, 2013.
13. Chen, B., Y.-C. Jiao, F.-C. Ren, L. Zhang, and F.-S. Zhang, "Design of open slot antenna for bandwidth enhancement with a rectangular stub," *Progress In Electromagnetics Research Letters*, Vol. 25, 109–115, 2011.
14. Liu, W. X., Y. Z. Yin, W. L. Xu, and S. L. Zuo, "Compact open-slot antenna with bandwidth enhancement," *IEEE Antennas and Wireless Propagation Letters*, Vol. 10, 850–853, 2011.
15. Song, K., Y. Z. Yin, X. B. Wu, and L. Zhang, "Bandwidth enhancement of open slot antenna with a T-shaped stub," *Microwave and Optical Technology Letters*, Vol. 52, 390–393, 2010.